

# ALMA OBSERVATION OF THE 658 GHz VIBRATIONALLY EXCITED H<sub>2</sub>O MASER IN ORION KL SOURCE I

TOMOYA HIROTA<sup>1,2</sup>, MI KYOUNG KIM<sup>3</sup>, MAREKI HONMA<sup>1,2</sup>

*Draft version January 13, 2016*

## ABSTRACT

We present an observational study of the vibrationally excited H<sub>2</sub>O line at 658 GHz ( $\nu_2=1$ ,  $1_{1,0}-1_{0,1}$ ) toward Orion KL using the Atacama Large Millimeter/Submillimeter Array (ALMA). This line is clearly detected at the position of the massive protostar candidate, the Source I. The spatial structure is compact with a size of about 100 AU and is elongated along the northeast-southwest low-velocity (18 km s<sup>-1</sup>) bipolar outflow traced by 22 GHz H<sub>2</sub>O masers, SiO masers, and thermal SiO lines. A velocity gradient can be seen perpendicular to the bipolar outflow. Overall spatial and velocity structure seems analogous to that of the 321 GHz H<sub>2</sub>O maser line previously detected with ALMA and vibrationally excited SiO maser emission. The brightness temperature of the 658 GHz H<sub>2</sub>O line is estimated to be higher than  $2 \times 10^4$  K, implying that it is emitted via maser action. Our results suggest that the 658 GHz H<sub>2</sub>O maser line is emitted from the base of the outflow from a rotating and expanding accretion disk as observed for the SiO masers and the 321 GHz H<sub>2</sub>O maser. We also search for two other H<sub>2</sub>O lines at 646 GHz (9<sub>7,3</sub>-8<sub>8,0</sub> and 9<sub>7,2</sub>-8<sub>8,1</sub>), but they are not detected in Orion KL.

*Subject headings:* ISM: individual objects (Orion KL) — ISM: molecules — masers — radio lines: ISM

## 1. INTRODUCTION

The Orion Kleinmann-Low (KL; Kleinmann & Low 1967) region is known as the nearest site of active massive-star formation at a distance of 420 pc (Menten et al. 2007; Kim et al. 2008). There are number of compact sources possibly associated with newly born young stellar objects (YSOs). The most dominant energy source is thought to be a radio source identified as Source I (Churchwell et al. 1987; Menten & Reid 1995). Because of its extremely high opacity at infrared wavelengths (Greenhill et al. 2004a; Sitarski et al. 2013), observational studies on Source I have been made mainly from centimeter to submillimeter wavelengths.

Observations with the Very Large Array (VLA) at 43 GHz resolve the continuum emission from Source I into a compact structure elongated in northwest-southeast direction with a major axis of  $\sim 100$  AU (Reid et al. 2007; Goddi et al. 2011). This emission can be explained by i) H<sup>-</sup> free-free radiation from optically thick neutral gas at  $< 4500$  K heated via mass accretion or ii) proton-electron free-free emission from compact HII region or from an ionized accretion disk with a higher temperature of  $\sim 8000$  K (Beuther et al. 2006; Reid et al. 2007; Goddi et al. 2011; Plambeck et al. 2013; Hirota et al. 2015). Recent studies favor the H<sup>-</sup> free-free radiation scenario (Reid et al. 2007; Plambeck et al. 2013; Hirota et al. 2015), while a luminosity of Source I required for the dynamical interaction scenario (see below) prefers the proton-electron free-free emission (Goddi et al. 2011). Future higher resolution observations at higher frequencies are required to decide between the two possibilities.

Proper motion measurements of Source I and the BN object, another high-mass YSO, with VLA have revealed that they are moving away from each other at a relative velocity of  $\sim 40$  km s<sup>-1</sup> (Gómez et al. 2008; Goddi et al. 2011). It is proposed that Source I and BN were ejected from a multiple system due to a dynamical interaction that occurred about 500 yrs ago (Goddi et al. 2011; Bally et al. 2011), and Source I formed a tight binary system with a total mass of  $20 M_{\odot}$ . At the same time, the dynamical decay released gravitational energy and ejected an explosive wide-angle outflow at an expansion velocity of  $> 100$  km s<sup>-1</sup> traced by the shocked H<sub>2</sub> and [Fe II] lines (Allen & Burton 1993; Kaifu et al. 2000; Bally et al. 2011, 2015), which largely provides the  $10^5 L_{\odot}$  luminosity of the KL nebula. It powers the strong (sub)millimeter line emission from the famous “hot core” (Beuther & Nissen 2008; Zapata et al. 2009b, 2011). On the other hand, there is an alternative explanation for the origin of the proper motions of this system (Tan 2004; Chatterjee & Tan 2012), in which the BN object was ejected 4500 yr ago by a dynamic interaction with the  $\theta^1$ C system in the Trapezium cluster rather than that with Source I. Therefore, such a dynamical interaction scenario is still a matter of debate.

Source I is also known as a driving source of another bipolar outflow along the northeast-southwest direction. The inner most part of the outflow at 10-100 AU scales is traced by vibrationally excited ( $v=1$ , 2) SiO masers (Menten & Reid 1995; Wright et al. 1995; Baudry et al. 1998; Greenhill et al. 1998; Doeleman et al. 1999, 2004; Greenhill et al. 2004b; Kim et al. 2008; Goddi et al. 2009; Matthews et al. 2010; Niederhofer et al. 2012a; Greenhill et al. 2013). Source I has been recognized as one of three rare YSOs displaying vibrationally excited SiO masers (Morita et al. 1992; Zapata et al. 2009a), suggesting a very large luminosity of  $> 10^4 L_{\odot}$ , as expected for late-type stars associated with SiO masers (Menten & Reid 1995). VLBI observations have revealed that the vibrationally excited SiO masers at 43 GHz

tomoya.hirota@nao.ac.jp

<sup>1</sup> National Astronomical Observatory of Japan, Osawa 2-21-1, Mitaka, Tokyo 181-8588, Japan

<sup>2</sup> Department of Astronomical Sciences, SOKENDAI (The Graduate University for Advanced Studies), Osawa 2-21-1, Mitaka, Tokyo 181-8588, Japan

<sup>3</sup> Korea Astronomy and Space Science Institute, Hwaam-dong 61-1, Yuseong-gu, Daejeon, 305-348, Republic of Korea

( $J=1-0$ ) trace the limb of an expanding, rotating disk seen edge-on that appears to be the base of a magnetically driven disk wind (Greenhill et al. 2004b; Matthews et al. 2010; Greenhill et al. 2013). They show a velocity gradient perpendicular to the outflow suggesting a rotating structure with an enclosed mass of  $\sim 7-8M_{\odot}$  (Kim et al. 2008; Matthews et al. 2010). This value is roughly consistent with that inferred from infrared spectroscopy of Source I, which suggests a  $10M_{\odot}$  protostar with a circumstellar disk (Testi et al. 2010), while it is significantly lower than that proposed by the dynamical interaction scenario, a  $20M_{\odot}$  binary (Goddi et al. 2011; Bally et al. 2011). The smaller mass estimates may provide a lower limit, if there is non-gravitational support such as radiation pressure and magnetic forces (Matthews et al. 2010).

Outside the vibrationally excited SiO maser distribution, the outflow can be traced by ground vibrational state ( $v=0$ ) SiO masers and 22 GHz  $H_2O$  masers on scales of 100-1000 AU (Genzel et al. 1981; Gaume et al. 1998; Hirota et al. 2007; Greenhill et al. 2013; Neufeld et al. 2013). Proper motion measurements of these maser features provide a 3-dimensional velocity field for the outflow with an expansion speed of  $\sim 18 \text{ km s}^{-1}$  (Genzel et al. 1981; Greenhill et al. 2013). This northeast-southwest outflow is sometimes called low-velocity ( $18 \text{ km s}^{-1}$ ) outflow. The outflow lobes continue to extend to larger than 1000 AU scales, traced by thermal SiO emission (Wright et al. 1995; Plambeck et al. 2009; Zapata et al. 2012; Niederhofer et al. 2012a) interacting with the ambient gas.

Recent observations with the Atacama Large Millimeter/Submillimeter Array (ALMA) have detected submillimeter  $H_2O$  lines at 321 GHz ( $10_{2,9}-9_{3,6}$ ) and 336 GHz ( $\nu_2=1, 5_{2,3}-6_{1,6}$ ) toward Source I (Hirota et al. 2014a). Maps of both these lines show velocities that are consistent with those of the SiO masers, i.e., a velocity gradient perpendicular to the bipolar outflow as seen in the SiO maser distributions. While the 321 GHz line emission is elongated along the bipolar outflow, the 336 GHz vibrationally excited line emission is unresolved with the ALMA beam size of  $0.4''$ . The velocity centroid map of the 336 GHz line is consistent with an origin in an edge-on rotating disk described above, i.e. a diameter of  $0.2''$  (84 AU) and an enclosed mass of  $>7M_{\odot}$ . The spectral profile of the 336 GHz line can be explained with an excitation temperature of  $>3000 \text{ K}$ , which is consistent with its lower state energy,  $E_l$ , of 2939 K. Thus, the 336 GHz line is consistent with thermal excitation, whereas the 321 GHz line could be a maser (Alcolea & Menten 1993). ALMA science verification (SV) data has also been used to detect the higher energy transition at 232 GHz ( $\nu_2=1, 5_{5,0}-6_{4,3}$ ) at a lower state energy level of  $E_l=3451 \text{ K}$  (Hirota et al. 2012). Although the spatial and velocity structure of the 232 GHz line was not resolved, due to its insufficient spatial resolution, detection of the high energy  $H_2O$  transition would imply evidence for a hot molecular gas component very close to the protostar candidate Source I (Reid et al. 2007; Testi et al. 2010).

The results discussed above demonstrate that the submillimeter  $H_2O$  lines at high excitation energy can play complementary roles to various SiO thermal and

maser lines and the 22 GHz  $H_2O$  maser, providing physical and dynamical properties of the hot molecular gas associated with newly born YSOs on a scale of  $\sim 100 \text{ AU}$ . However, the physical properties and dynamical structure of the  $H_2O$  emission region have not been fully understood yet, owing to the limited amount high resolution data (Hunter et al. 2007; Patel et al. 2007; Hirota et al. 2012; Niederhofer et al. 2012b; Hirota et al. 2014a; Richards et al. 2014).

In this paper, we report ALMA observations of the vibrationally excited  $H_2O$  line at 658 GHz toward Orion KL Source I. The 658 GHz  $H_2O$  line is the lowest rotational transition at the first vibrationally excited state of the ortho  $H_2O$  ( $\nu_2=1, 1_{1,0}-1_{0,1}$ ), with a lower state energy level of  $E_l=2329 \text{ K}$  (Chen et al. 2000). The 658 GHz  $H_2O$  maser lines has been detected toward late-type stars by the Caltech Submillimeter Observatory (CSO) 10.4 m telescope (Menten & Young 1995), the Submillimeter Array (SMA) (Hunter et al. 2007), and the recently released ALMA SV data (Richards et al. 2014). However, it is not seen toward the star-forming regions W49N and W51 IRS2 (Menten & Young 1995), in spite of their extremely strong 22 GHz  $H_2O$  maser emissions. The 658 GHz  $H_2O$  line was identified in a single-dish line survey toward the Orion KL with the CSO 10.4 m telescope (Schilke et al. 2001). However, its position and source size could not be determined, because of the large beam size of the single-dish telescope  $\sim 10''$ . We present high resolution imaging of the 658 GHz  $H_2O$  lines for the first time in star-forming region with a spatial resolution of  $\sim 0.26''$  or 100 AU. The compact structure and high flux density suggest that the 658 GHz line is showing maser action. Given that SiO and  $H_2O$  are the only molecules from which emission has been detected toward Source I, further high-resolution, multi-transition studies of vibrationally excited  $H_2O$  lines (e.g. Humphreys 2007) will greatly contribute to our understanding of the structure and dynamics of disk/outflow systems associated with this highly interesting object.

## 2. OBSERVATIONS

Observations with ALMA at band 9 were carried out during Cycle 0 at five epochs (ADS/JAO.ALMA#2011.00199.S). Among them, we selected the Aug. 25, 2012 observation for analysis in the present paper, as it contained the most antennas, longest baselines, and most on-source time. Total on-source time was 350 seconds, consisting of 6 scans of 30 or 72 seconds every 10 minutes, and the maximum baseline length was 385 m (845 k $\lambda$ ). The UV coverage for this session is shown in Figure 1. Because of the lack of visibility data at 658 GHz and/or large flux uncertainties from epoch to epoch as discussed later, we did not combine multiple epoch data. Typical system noise temperatures were about 1400 K at 658 GHz.

The tracking center position of Orion KL was adopted from the 22 GHz  $H_2O$  supermaser, RA(J2000)=05h35m14s.1250, Decl(J2000)=05d22'36".486 (Hirota et al. 2011, 2014b). Because the original target of our ALMA Cycle 0 project was the supermaser, Source I was detected serendipitously. It is located at ( $5.8''$ ,  $5.9''$ ) northeast of the tracking center position, and hence, outside the primary beam size of the ALMA 12 m antenna,  $9.4''$  at 658 GHz (Figure 2).

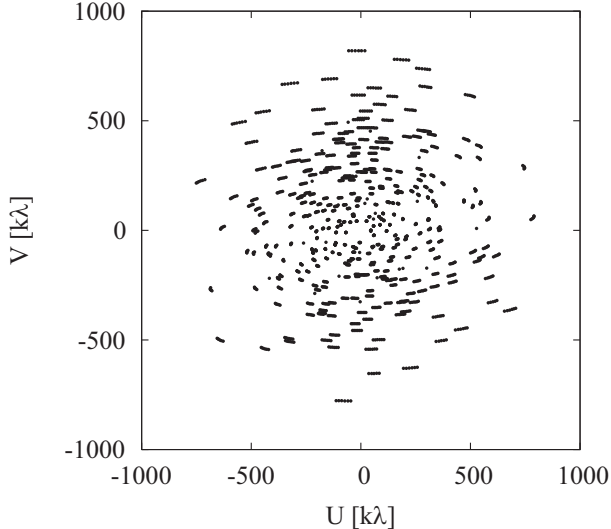


FIG. 1.— UV coverage of the ALMA observation at band 9 on Aug. 25, 2012.

Bandpass, flux, and gain calibrators were J0423-013, Callisto, and J0607-085, respectively.

We observed four spectral windows (spw) in band 9 with bandwidths of 938 MHz for both of the linear polarizations. The spw centered at 658.2 GHz included the  $\nu_2=1$ ,  $1_{1,0}-1_{0,1}$  line of  $\text{H}_2\text{O}$  at a rest frequency of 658.006550 GHz (Chen et al. 2000). We also observed other  $\text{H}_2\text{O}$  lines at 645.766010 GHz ( $9_{7,3}-8_{8,0}$ ) and 645.950620 GHz ( $9_{7,2}-8_{8,1}$ ) in the vibrationally ground state, with a lower state energy of  $E_l=2574$  K (Chen et al. 2000), which were in another spw centered at 646.8 GHz. However, we could not detect these two lines with an rms noise level ( $1\sigma$ ) of  $\sim 1$  Jy beam. Two other spws at 640.6 GHz and 662.2 GHz were used for continuum emission. The spectral resolution and number of spectral channels were 244 kHz and 3840 channels, respectively. The corresponding velocity resolution was  $0.11 \text{ km s}^{-1}$  at 658 GHz.

### 3. DATA ANALYSIS

Synthesis imaging and self-calibration were done using the Common Astronomy Software Applications (CASA) package in a standard manner<sup>4</sup>. Part of the data plotting and image analysis were made by using the Astronomical Image Processing System (AIPS) package. We used the calibrated visibility data delivered by the East Asia ALMA Regional Center (EA-ARC) to make synthesized images. We first conducted Doppler tracking with the CASA task `cvel`, setting the rest frequency to 658.006550 GHz. Next we identified line-free channels and subtracted the continuum emission from the calibrated visibility data using the CASA task `uvcontsub3`.

Self-calibration was done for the peak channel of the  $\text{H}_2\text{O}$  line at the LSR (Local Standard of Rest) velocity of  $13.0 \text{ km s}^{-1}$  with the CASA task `clean` and `gaincal`. First we solved only for phase solutions, with a short integration time of 5 seconds. We then self-calibrated the data with longer integration times (30 or 72 seconds) and solved for both phase and amplitude solutions.

These phase and amplitude solutions were applied to rest of the spectral channels, including other spws for continuum data by using the CASA task `applycal`. The resultant rms noise level for each line-free channel was  $1.2 \text{ Jy beam}^{-1}$  ( $1\sigma$ ) at 658 GHz, although it increases to  $1.6 \text{ Jy beam}^{-1}$  ( $1\sigma$ ) at the channels with significant emission. The synthesized beam size was  $0.28'' \times 0.25''$  at a position angle of  $-64$  degrees using natural weighting. Because the baseline length ranged from 21-385 m ( $45-845 \text{ k}\lambda$ ), extended structures of  $>5''$  are resolved out.

Applying the self-calibration solutions to all of the spectral channels and spws, we produced a spectral line data cube with a channel spacing of  $0.11 \text{ km s}^{-1}$ . For illustration purpose, we also made a lower-resolution channel map by integrating 9 velocity channels ( $\sim 1 \text{ km s}^{-1}$ ) as shown in Figure 3. The moment 0 and 1 maps were made using the CASA task `immoments` (Figure 4).

By using the line-free channels, we also made a synthesis image of the continuum emission of this region. As shown in Figure 2(b), we detected Source I and some other compact sources possibly corresponding to the main dust ridge, compact ridge, and other compact radio/infrared sources (Greenhill et al. 2004a; Favre et al. 2011; Friedel & Widicus Weaver 2011; Sitarski et al. 2013; Plambeck et al. 2013; Hirota et al. 2015). Interpretation is not straightforward as our image can retrieve only a small fraction of the total (large scale) continuum emission which is “resolved out” by ALMA. This also produces imaging artifacts. A brief summary of the continuum emission is given in Section 4.5, although detailed discussion is beyond the scope of this paper.

#### 3.1. Flux density scale and its uncertainty

Here we discuss the flux density scale and its uncertainty caused by two major factors. Firstly, we estimate the flux scale affected by the primary beam correction. The target source, Source I is located outside the FWHM of the primary beam of the ALMA 12 m antenna of  $9.4''$  as described above. The position offset is ( $5.8''$ ,  $5.9''$ ) northeast of the tracking center position. If we consider a possible pointing error of  $0.6''$  as described in the ALMA Cycle 0 Technical Handbook<sup>6</sup>, the primary beam correction factor for Source I is estimated to be  $8.6^{+3.3}_{-2.2}$ . Thus, the flux uncertainty is  $\sim 40\%$ .

Next, we consider other sources of uncertainty in the absolute flux calibration. We find that a flux density variation of the gain calibrator J0607-085 among four spws range from 0.64 Jy to 1.51 Jy in this epoch. The mean and standard deviation of the flux density of J0607-085 are 1.12 Jy and 0.36 Jy, respectively, suggesting that an additional flux calibration error of 30%. This value is larger than the absolute flux calibration accuracy presented in the ALMA Cycle 0 Technical Handbook of 20%. We find less flux density variation in another epoch on July 17 ranging from 0.61 to 0.66 Jy, although these data are not employed in this paper. Their mean and standard deviation are 0.63 Jy and 0.02 Jy, respectively. This value is consistent with that of the lowest value for one of the spws in Aug. 25 of 0.64 Jy. Because the spw including the 658 GHz  $\text{H}_2\text{O}$  line shows the highest flux density of 1.51 Jy on Aug. 25, the flux calibration for the 658 GHz

<sup>5</sup> [https://casaguides.nrao.edu/index.php/Main\\_Page](https://casaguides.nrao.edu/index.php/Main_Page)

<sup>6</sup> [http://almascience.eso.org/documents-and-tools/cycle-0/alma-technical-handbook/at\\_download/file](http://almascience.eso.org/documents-and-tools/cycle-0/alma-technical-handbook/at_download/file)

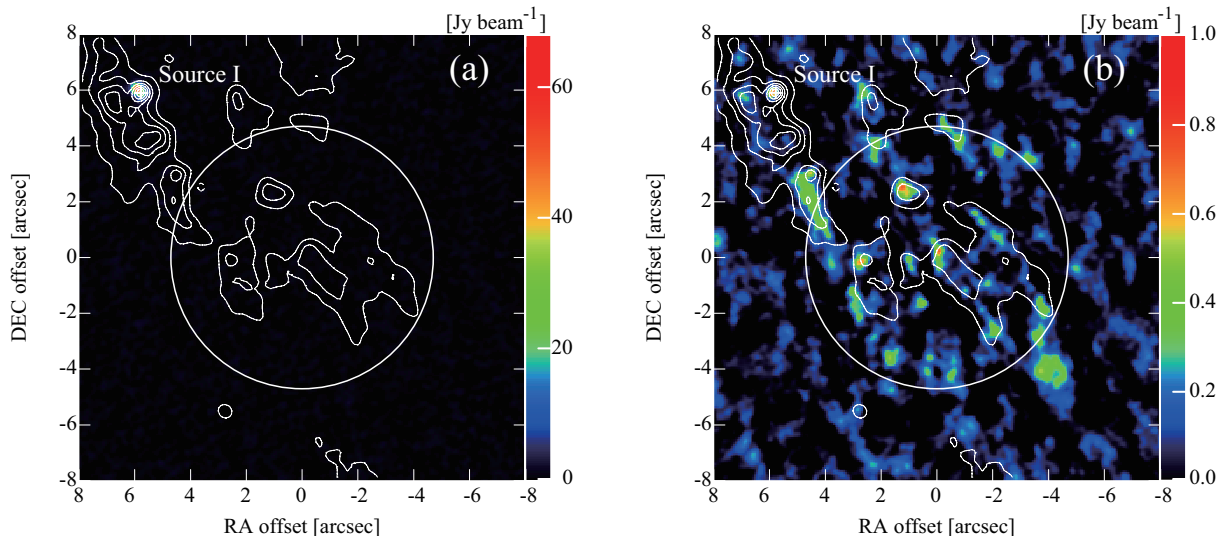


FIG. 2.— Maps of the Orion KL region with the position of Source I indicated. Contours show the distribution of ALMA band 7 (339 GHz) continuum emission (Hirota et al. 2015). The contours start at  $-5\sigma$  level with an interval of  $10\sigma$  ( $-5, 5, 15, 25, \dots$ ) with a  $1\sigma$  level of  $9 \text{ mJy beam}^{-1}$ . A white circle indicates the half-power beam width (primary beam size) of an ALMA 12 m antenna at band 9 of  $9.4''$ . (a) The intensity distribution of the 658 GHz  $\text{H}_2\text{O}$  line at the peak LSR (Local Standard of Rest) velocity channel of  $13.0 \text{ km s}^{-1}$  is shown by a color image. (b) A band 9 continuum image is shown in color. The primary beam attenuation for ALMA band 9 data is not corrected for in either panel.

$\text{H}_2\text{O}$  line could be overestimated by a factor of 2.4 on Aug. 25. The possible flux calibration error at 658 GHz could be affected by the larger atmospheric opacity close to the 658 GHz  $\text{H}_2\text{O}$  line and/or the 656 GHz  $\text{O}_3$  line (Schilke et al. 2001). In this paper, we employ the absolute flux density of J0607-085 to be  $0.64 \text{ Jy}$ . We correct this spw-to-spw flux variation for the 658 GHz line by a factor of  $0.64/1.51=0.42$ . This may underestimate the flux density of the 658 GHz  $\text{H}_2\text{O}$  line by a factor of 0.42 at maximum if the actual flux density of J0607-085 is  $1.51 \text{ Jy}$ .

In summary, the total flux calibration uncertainty is  $\sim 50\%$  for both of the 658 GHz  $\text{H}_2\text{O}$  line and continuum data, while the absolute flux scale of the 658 GHz line could be underestimated by a factor of 0.42.

### 3.2. Absolute and relative positional accuracy

We measured the position of Source I using the band 9 continuum map (Figure 2) by fitting a single Gaussian with the CASA task `imfit`. The measured position of Source I is listed in Table 1. A typical formal error in the Gaussian fitting is  $5 \text{ mas}$  as indicated in the Table 1. We note that this does not include a systematic error term for the absolute astrometry. For comparison, we also list the predicted position of Source I based on accurate absolute astrometry of the VLA 43 GHz data (Goddi et al. 2011). The errors for the VLA data in Table 1 include those of proper motion and absolute positional accuracy of  $\sim 5 \text{ mas}$  (Goddi et al. 2011). We find that the position offset of the band 9 continuum relative to the VLA 43 GHz data are  $40 \text{ mas}$  and  $20 \text{ mas}$  in right ascension and declination, respectively. These values could be the absolute position uncertainty in the continuum observations of Source I at ALMA band 9. Possible source of astrometric error include a contribution from poorly imaged (see above) extended structure of the hot core and main dust ridge (Hirota et al. 2015), uncertainties in primary beam attenuation of the images, and calibration

errors.

As discussed above, we applied the phase and amplitude calibration solutions to all spws. This allows us to register the 658 GHz  $\text{H}_2\text{O}$  map and that of the band 9 continuum emission. Thus, the error in the relative positions between the 658 GHz  $\text{H}_2\text{O}$  line and band 9 continuum should be determined by the signal-to-noise ratio and the beam size. As listed in Table 1, the relative positional error of the ALMA band 9 continuum and the moment 0 map of the 658 GHz  $\text{H}_2\text{O}$  line is  $7 \text{ mas}$ , obtained from the formal errors in the Gaussian fitting.

For each velocity channel map of the 658 GHz  $\text{H}_2\text{O}$  line emission, we performed a two dimensional Gaussian fit to determine peak positions using the AIPS task SAD (e.g. Figure 5(a)). At the peak velocity channel of the 658 GHz  $\text{H}_2\text{O}$  line, the signal-to-noise ratio is  $\sim 100$ , and hence, the positional precision is estimated to be  $\sim 0.002''$ . Errors in the Gaussian fitting which range from  $0.001''$  to  $0.05''$  ( $1\sigma$ ) with the typical value of  $0.01''$  are consistent with this estimate. Because some of the channel maps clearly show spatial structure indicative of multiple components and/or structure larger than the beam size of  $\sim 0.26''$ , a single Gaussian model may result in larger positional uncertainties.

In summary, the absolute position uncertainty of Source I in the present ALMA band 9 continuum observations is  $\sim 50 \text{ mas}$ , and the relative positional errors between the band 9 continuum and  $\text{H}_2\text{O}$  lines are  $1\text{--}50 \text{ mas}$  depending on the source structure and signal-to-noise ratio.

## 4. RESULTS AND DISCUSSION

### 4.1. Spatial structure

Figure 3 shows channel maps of the 658 GHz  $\text{H}_2\text{O}$  line smoothed to a velocity width of  $1 \text{ km s}^{-1}$ . The systemic velocity of Source I is  $v_{\text{LSR}}=5 \text{ km s}^{-1}$  (e.g. Plambeck et al. 1990). As can be seen in Figures 2 and 3, the emission of the 658 GHz line is concentrated only

TABLE 1  
POSITION AND SIZE OF SOURCE I

Tracer	$\alpha$ (J2000)	$\delta$ (J2000)	FWHM("×") <sup>a</sup>	PA (deg.)	Reference
658 GHz H <sub>2</sub> O line (moment 0)	05h35m14s.5164(3)	-05d22'30".491(5)	0.525(10)×0.384(9)	44.6(12)	
Band 9 continuum	05h35m14s.5182(4)	-05d22'30".537(5)	0.345(10)×0.269(10)	155(3)	
VLA 43 GHz continuum	05h35m14s.5156(4)	-05d22'30".560(6)	...	...	Goddi et al. (2011)

NOTE. — For ALMA band 9 data, positions and sizes are measured by a single Gaussian fitting. Numbers in parenthesis represent fitting errors determined by the CASA task `imfit` in units of the last significant digit. Errors do not include astrometric uncertainties of 40 mas and 20 mas in right ascension and declination, respectively. For the VLA 43 GHz continuum, the absolute position is calculated from that in 2009 January 12 and corrected for the measured proper motion to the epoch of the ALMA data (Goddi et al. 2011). Numbers in parenthesis represent errors that include both the absolute astrometry and proper motion uncertainties in units of the last significant digit.

<sup>a</sup> Convolved with a synthesized beam of  $0.28'' \times 0.25''$  with a position angle of  $-64$  deg.

around Source I, and the spatial distribution is compact with a size of less than  $1''$ . Each channel map reveals a slightly more extended feature than that of the beam size,  $\sim 0.26''$  or 100 AU. The compact distribution toward Source I is similar to those observed for the 321 GHz and 336 GHz H<sub>2</sub>O lines (Hirota et al. 2014a). In contrast, it is quite different from that of the well studied 22 GHz H<sub>2</sub>O maser and the 325 GHz submillimeter H<sub>2</sub>O maser, which are distributed along a bipolar outflow on a much larger scale of  $>1000$  AU (Genzel et al. 1981; Gaume et al. 1998; Hirota et al. 2007; Niederhofer et al. 2012b; Greenhill et al. 2013; Neufeld et al. 2013). This is because the 22 GHz and 325 GHz H<sub>2</sub>O masers have the significantly different excitation requirements with the lower state energy levels of 642 K and 454 K, respectively, much lower than the values for the 658, 321 and 336 GHz lines (Chen et al. 2000). The higher excitation lines at 658 GHz, 321 GHz, and 336 GHz trace a denser and hotter region close vicinity to Source I.

Figure 4 shows the moment 0 and 1 maps of the 658 GHz H<sub>2</sub>O line. The spatial distribution is elongated along the northeast-southwest direction with the size of  $0.525'' \times 0.384''$  or  $\sim 220$  AU  $\times$  160 AU. The elongation of the moment 0 map indicates that the 658 GHz H<sub>2</sub>O line should be related to the low-velocity ( $18 \text{ km s}^{-1}$ ) outflow along the same direction. A velocity gradient is clearly seen perpendicular to the elongation, similar to the vibrationally excited SiO masers (Kim et al. 2008; Matthews et al. 2010). These characteristics are also analogous to that of the 321 GHz H<sub>2</sub>O maser line (Hirota et al. 2014a). The position angle of the moment 0 map of the 658 GHz H<sub>2</sub>O line,  $44.6 \pm 1.2$  degrees (Table 1), is slightly smaller than that measured both from emission locus and proper motions of the ground vibrational state SiO masers,  $56 \pm 1$  degrees (Greenhill et al. 2013). This difference is probably due to the asymmetric brightness distribution of the 658 GHz H<sub>2</sub>O line, where the red-shifted component of the 658 GHz H<sub>2</sub>O line is dominant compared with the blue-shifted one (as seen in the channel map in Figure 3).

We present a velocity centroid map of the 658 GHz H<sub>2</sub>O line (Figure 5) to compare with those of other submillimeter H<sub>2</sub>O lines and the 43 GHz SiO masers (Kim et al. 2008; Hirota et al. 2014a). All of the map centers are registered to the peak positions of the continuum emission of Source I at each frequency band. The spatial distribution of the 658 GHz H<sub>2</sub>O line map shows an “M-shaped” distribution with a position angle of  $\sim 45$  degrees as seen in Figure 5(a) and is slightly different from those of the 321 GHz H<sub>2</sub>O maser line

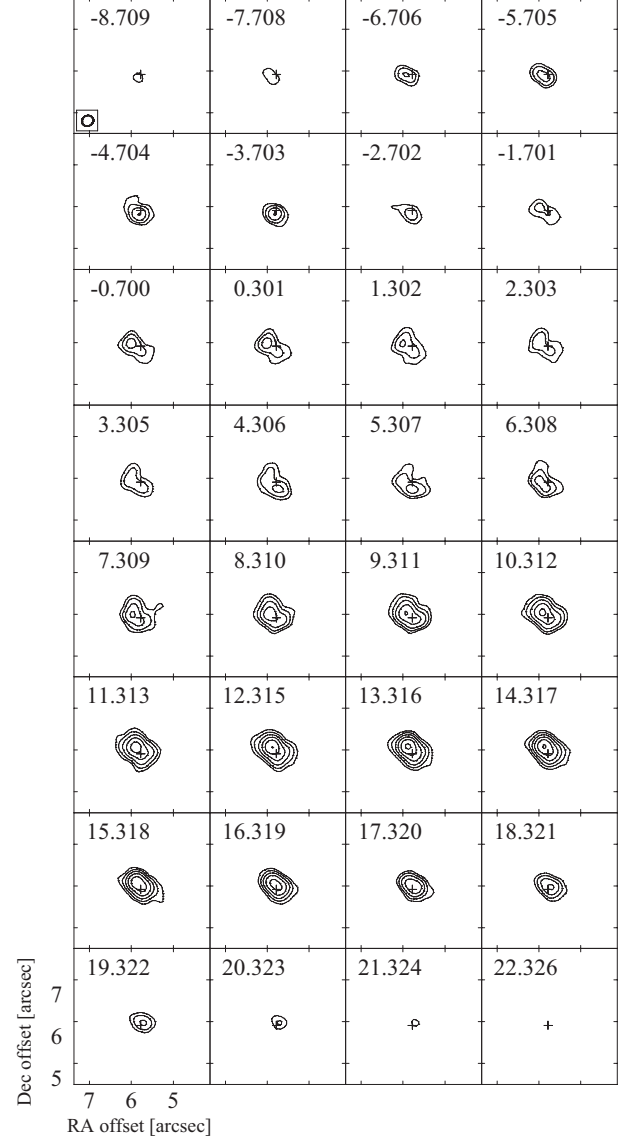


FIG. 3.— Channel map of the 658 GHz H<sub>2</sub>O line. The map is smoothed with the velocity width of  $1 \text{ km s}^{-1}$  for illustration purpose. The LSR velocity of the map is indicated in each panel. The systemic velocity of Source I is  $v_{LSR} = 5 \text{ km s}^{-1}$ . The contour levels are  $25 \text{ Jy beam}^{-1}$  ( $1\sigma$ ) times  $-5, 5, 10, 20, 40, 80$ , and  $160$ . A cross represents the position of the band 9 continuum emission peak of Source I. A synthesized beam,  $0.28'' \times 0.25''$  with a position angle of  $-64$  degrees, is shown at the bottom-left corner of the first panel ( $-8.7 \text{ km s}^{-1}$ ). Corrections for primary beam attenuation and spw-to-spw flux variation have been applied.



(Hirota et al. 2014a) and SiO masers observed with connected arrays (Menten & Reid 1995; Wright et al. 1995; Baudry et al. 1998; Goddi et al. 2009; Niederhofer et al. 2012a). However, the overall shape of the 658 GHz  $\text{H}_2\text{O}$  map is not very different from that of the 321 GHz maser line, showing two parallel structure along the northwest-southeast directions. On the other hand, the velocity centroid map of the 658 GHz  $\text{H}_2\text{O}$  line is strikingly different from that of the 336 GHz vibrationally excited  $\text{H}_2\text{O}$  line (Hirota et al. 2014a), which shows a linear spatial distribution perpendicular to the two ridge-like structure of the 658 GHz and 321 GHz  $\text{H}_2\text{O}$  maps. Between the two ridge-like structure, there is a cluster of the SiO masers detected by VLBI (Kim et al. 2008). The sizes of the 321 GHz, 336 GHz, and 658 GHz  $\text{H}_2\text{O}$  line emission, as well as the vibrationally excited SiO masers, are comparable with each other.

The distributions of the submillimeter  $\text{H}_2\text{O}$  lines in Source I appear to be different from those of the red supergiant VY CMa observed with ALMA (Richards et al. 2014). The inner rims of the 658 GHz and 321 GHz  $\text{H}_2\text{O}$  maser shells around VY CMa are distributed at successively larger distances from the star's position, while they are outside the SiO maser shell (Richards et al. 2014). Furthermore, the size of the outer rim of the distribution of the 321 GHz  $\text{H}_2\text{O}$  maser emission is larger than that of the 658 GHz masers by a factor of 2 (200 mas and 500 mas, respectively). Such different distributions are not apparent in Source I. Although the angular resolution of their observations, ( $0.18'' \times 0.09''$  and  $0.088'' \times 0.044''$  at 321/325 GHz and 658 GHz respectively) are smaller than that of our observation, the spatial resolutions on a linear scale are comparable,  $\sim 100$  AU. We cannot rule out a possibility that the apparent structure in the velocity centroid map of Source I could be an artifact caused by the insufficient spatial resolution as suggested by the SiO maser data (Goddi et al. 2009). Further observational studies at higher spatial resolution with ALMA are crucial to reveal the smaller scale  $\text{H}_2\text{O}$  maser structure of Source I.

#### 4.2. Spectral profile

Figure 6 shows the spectral profile of the 658 GHz  $\text{H}_2\text{O}$  line along with other  $\text{H}_2\text{O}$  lines (Hirota et al. 2012, 2014a). The peak flux density is 940 Jy at the LSR velocity of  $13.0 \text{ km s}^{-1}$ . The source size of the 658 GHz  $\text{H}_2\text{O}$  channel map at  $13.0 \text{ km s}^{-1}$  is derived to be  $0.42'' \times 0.31''$  by the two-dimensional Gaussian fitting of the image. The brightness temperature of the 658 GHz  $\text{H}_2\text{O}$  line is calculated to be  $2 \times 10^4 \text{ K}$  or higher, as the emission region is unresolved with the ALMA beam. Even this value may be underestimated by a factor of  $1/0.42$  as discussed in Section 3.1. The observed high brightness temperature implies that maser action as a possible emission mechanism for the 658 GHz  $\text{H}_2\text{O}$  line.

The 658 GHz  $\text{H}_2\text{O}$  line has been detected by the 10.4 m single-dish telescope of the CSO (Schilke et al. 2001) with the beam size of  $10''$ . The main-beam brightness temperature of the CSO observation is  $T_R^* = 8.9 \text{ K}$  corresponding to the total flux density of 300 Jy. This value is smaller than our ALMA results by a factor of 3. The difference could be explained neither by the calibration

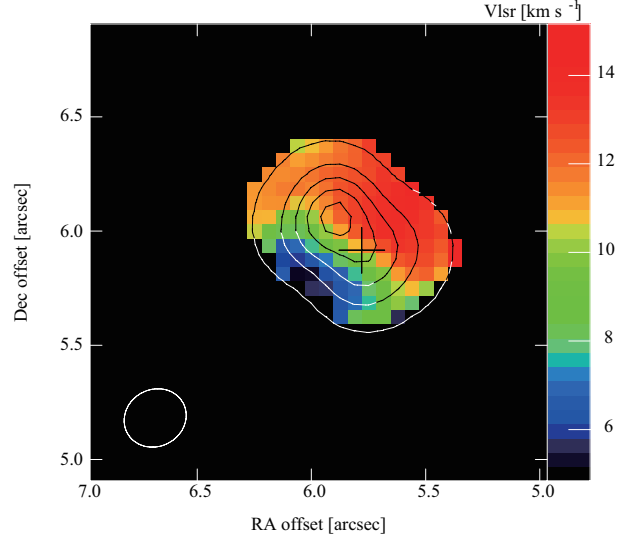


FIG. 4.— Moment 0 (contour) and 1 (color) maps of the 658 GHz  $\text{H}_2\text{O}$  line emission. The contour levels are 10%, 30%, 50%, 70%, and 90% of the peak intensity of  $3923 \text{ Jy beam}^{-1} \text{ km s}^{-1}$ . A black cross corresponds to the position of Source I determined by the continuum peak position. A synthesized beam size is shown in the bottom-left corner. Primary beam attenuation and spw-to-spw flux variation factors have been corrected. The systemic velocity of Source I is  $v_{LSR} = 5 \text{ km s}^{-1}$ , which is offset from the central velocity of the plotting range (i.e.  $10 \text{ km s}^{-1}$  as indicated by green).

error ( $\sim 50\%$ ) and pointing offset of the CSO data<sup>8</sup> nor the calibration uncertainty of the ALMA data. It may suggest a flux variation of the 658 GHz  $\text{H}_2\text{O}$  maser line, although further accurate flux monitoring with ALMA are still necessary to confirm this hypothesis.

For comparison, we also present the other  $\text{H}_2\text{O}$  lines detected with previous ALMA observations (Hirota et al. 2012, 2014a) in Figure 6. Double-peaked spectral profiles showing brighter red-shifted component are common for all lines, except the 336 GHz line which shows a symmetric line profile. Nevertheless, the peak velocities of these double-peaked components are almost the same for all the lines. These double-peaked structures are also consistent with those of various SiO maser lines detected with the VLA (Goddi et al. 2009), as shown in Figure 6. The observed line profiles, along with the similar distribution of the  $\text{H}_2\text{O}$  lines at 232 GHz, 321 GHz, and 658 GHz, support the idea that these lines are emitted under similar excitation conditions.

#### 4.3. Excitation condition of the 658 GHz $\text{H}_2\text{O}$ line

Based on the spatial structure and spectral profiles, it is most likely that the 658 GHz  $\text{H}_2\text{O}$  line is associated with the base of the outflow as revealed by VLBI observations of SiO masers (Greenhill et al. 2004b; Kim et al. 2008; Matthews et al. 2010) and the 321 GHz  $\text{H}_2\text{O}$  maser line (Hirota et al. 2014a). The brightness temperature of the 658 GHz  $\text{H}_2\text{O}$  line,  $> 2 \times 10^4 \text{ K}$ , would indicate that the line is emitted via maser action. In contrast, the 336 GHz  $\text{H}_2\text{O}$  line shows a different distribution (Figure 5(c)) and a spectral profile with symmetric double-peaks

<sup>9</sup> The CSO observation by Schilke et al. (2001) was carried out toward the hot core position at the position of RA(J2000)=05h35m14s.5, Decl(J2000)=−05d22′31″.

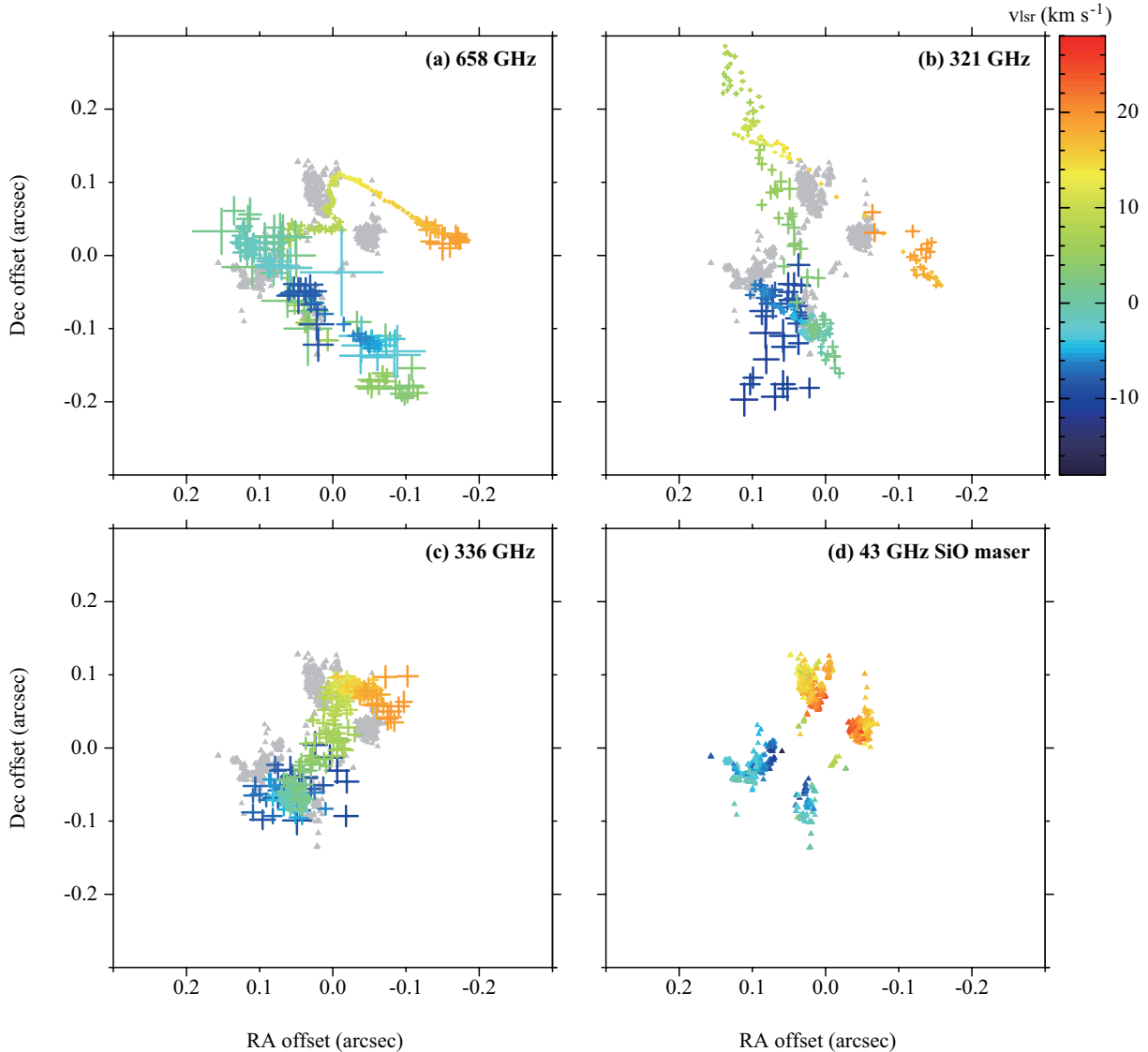


FIG. 5.— Velocity centroid maps of (a) the 658 GHz  $\text{H}_2\text{O}$  line, (b) the 321 GHz  $\text{H}_2\text{O}$  line, (c) the 336 GHz  $\text{H}_2\text{O}$  line, and (d) the 43 GHz SiO masers (Hirota et al. 2014a). Colors indicate the LSR velocity. The systemic velocity of Source I is  $v_{\text{LSR}} = 5 \text{ km s}^{-1}$ . Each cross indicates a peak position with its formal error from Gaussian fitting. Triangles represent the positions of the SiO maser spots (Kim et al. 2008). In panels (a), (b), and (c), the SiO maser positions are indicated by gray symbols.

(Figure 6). As discussed in Alcolea & Menten (1993) and Hirota et al. (2014a), the 336 GHz  $\text{H}_2\text{O}$  line could be a thermal line and trace the edge-on disk, unlike emission from the other transitions at 232 GHz, 321 GHz, and 658 GHz. We note that Menten et al. (2006) the 336 GHz  $\text{H}_2\text{O}$  line toward the red supergiant VY CMa also favor a thermal nature for this line’s excitation.

Recently, theoretical model calculations for the excitation of the 658 GHz  $\text{H}_2\text{O}$  line have been presented (Richards et al. 2014; Nesterenok 2015) for the red supergiant VY CMa and for asymptotic giant branch (AGB) stars. The 658 GHz  $\text{H}_2\text{O}$  maser is predicted to be pumped efficiently for an  $\text{H}_2$  densities of  $10^9$ - $10^{10} \text{ cm}^{-3}$ , a fractional  $\text{H}_2\text{O}$  abundance of  $10^{-4}$ - $10^{-5}$ , and gas temperatures of 1000-1500 K (Nesterenok 2015). Although the physical and chemical properties of the 658 GHz  $\text{H}_2\text{O}$  maser emitting region associated with Source I would be expected to be different from that of a late-type star,

these parameters are roughly consistent with those for the disk-outflow system of Source I associated with SiO masers and other submillimeter  $\text{H}_2\text{O}$  lines (Reid et al. 2007; Goddi et al. 2009, 2011; Hirota et al. 2014a, 2015).

#### 4.4. Relationship between the 22 GHz $\text{H}_2\text{O}$ supermaser

We note that our ALMA observation was done during an active phase of the 22 GHz  $\text{H}_2\text{O}$  maser burst in Orion KL, called a “supermaser” (Hirota et al. 2011, 2014b). The 22 GHz supermaser is located at the phase tracking center of the ALMA observation, corresponding to the Compact Ridge region (Hirota et al. 2011, 2014b). While the total flux density of the 22 GHz  $\text{H}_2\text{O}$  supermaser was decreasing on August 25, 2012, it was still  $\sim 2 \times 10^4 \text{ Jy}$  (Hirota et al. 2014b). In spite of the extremely high flux density of this maser, there was no significant emission of the 658 GHz  $\text{H}_2\text{O}$  line in the Compact Ridge region in our ALMA data with the  $1\sigma$  noise level of

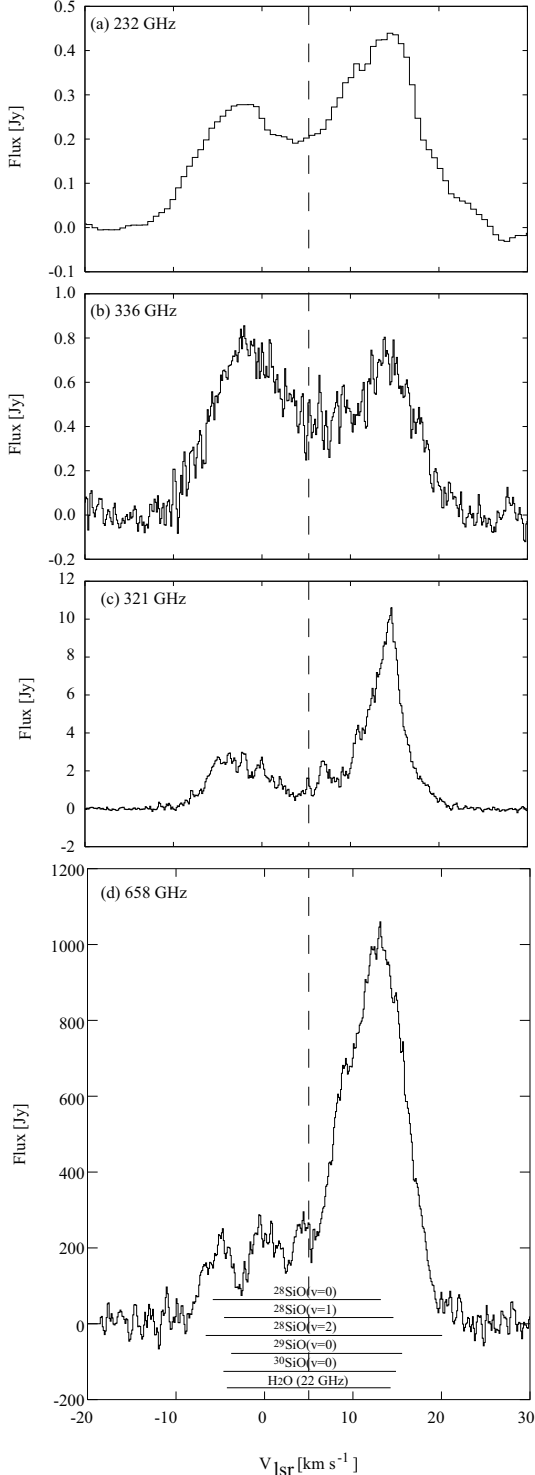


FIG. 6.— Spectra of the millimeter and submillimeter  $\text{H}_2\text{O}$  lines. (a) 232 GHz ( $\nu_2=1$ ,  $5_{5,0}-6_{4,3}$ ) line taken from the ALMA SV data at band 6 (Hirota et al. 2012). (b) 336 GHz ( $\nu_2=1$ ,  $5_{2,3}-6_{1,6}$ ) line observed in ALMA Cycle 0 at band 7 (Hirota et al. 2014a). (c) 321 GHz ( $10_{2,9}-9_{3,6}$ ) line observed in ALMA Cycle 0 at band 7 (Hirota et al. 2014a). (d) 658 GHz ( $\nu_2=1$ ,  $1_{1,0}-1_{0,1}$ ) line. Primary beam attenuation and spw-to-spw flux variation factors have been corrected. The velocity ranges between the blue-shifted and red-shifted peaks for SiO (Goddard et al. 2009) and 22 GHz  $\text{H}_2\text{O}$  (Gaume et al. 1998) spectra are shown by horizontal bars. The systemic velocity of Source I is  $v_{LSR}=5 \text{ km s}^{-1}$ , as indicated by a vertical dashed line.

$2 \text{ Jy beam}^{-1}$  in the relevant region. Thus, the 658 GHz  $\text{H}_2\text{O}$  line is not related to the 22 GHz supermaser phenomenon, as has also been reported for other transition at 321 GHz and 336 GHz (Hirota et al. 2014b).

#### 4.5. Continuum emission at ALMA band 9

To measure the position of the 658 GHz  $\text{H}_2\text{O}$  emission, we also made a map of the ALMA band 9 continuum by applying the self-calibration solutions. Continuum emission is detected at the position of Source I, although it is outside the primary beam of the 12 m antenna. The flux density and the peak intensity are derived from Gaussian fitting,  $1.04 \pm 0.04 \text{ Jy}$  and  $0.77 \pm 0.03 \text{ Jy beam}^{-1}$ , respectively (Figure 2(b)). If we correct the primary beam attenuation by a factor of 8.6, the absolute flux density is calculated to be  $8.9 \text{ Jy}$ , with an uncertainty of 50%. This value is slightly larger than that of the SMA observation at 690 GHz,  $6.7 \pm 3.2 \text{ Jy}$  (Beuther et al. 2006), but within the mutual errors. The apparent source size is almost comparable to the beam size as listed in Table 1, and hence, the continuum emission of Source I is unresolved with our ALMA observation. Due to the large ( $\sim 50\%$ ) flux uncertainty of Source I (which is outside the primary beam), the limited field of view, and insufficient image quality in particular for spatially extended components, we will not discuss detailed properties of the continuum emission of Source I.

#### 5. SUMMARY

By using ALMA Cycle 0 data, we detect the 658 GHz  $\text{H}_2\text{O}$  line toward the massive protostar candidate Source I in the Orion KL region. The 658 GHz  $\text{H}_2\text{O}$  line is emitted from a compact structure with the size of  $\sim 100 \text{ AU}$ . The source structure is elongated along the northeast-southwest direction parallel to the low-velocity ( $18 \text{ km s}^{-1}$ ) molecular outflow. A velocity gradient can be seen along the northwest-southeast direction, which is perpendicular to the outflow axis and the source elongation. The spectral profile represents a double-peaked structure, similar to the other millimeter/submillimeter  $\text{H}_2\text{O}$  lines at 232 GHz and 321 GHz lines (Hirota et al. 2012, 2014a). The high brightness temperature of  $> 2 \times 10^4 \text{ K}$  is consistent with maser emission. These basic properties would suggest that the 658 GHz  $\text{H}_2\text{O}$  line is emitted from the base of the northeast-southwest low-velocity ( $18 \text{ km s}^{-1}$ ) molecular outflow. Further multi-transition studies of the  $\text{H}_2\text{O}$  lines with ALMA at higher spatial resolution should provide information about the excitation mechanism and physical properties of the millimeter and submillimeter  $\text{H}_2\text{O}$  line emissions. They will be powerful tools to investigate dynamics, physics and chemistry in outflow launching regions associated with accretion disks around massive YSOs, which is a key issue to understand formation mechanisms of massive YSOs.

We acknowledge Karl M. Menten and Mark J. Reid for a critical reading of the manuscript. This paper makes use of the following ALMA data: ADS/JAO.ALMA#2011.0.00199.S. ALMA is a partnership of ESO (representing its member states), NSF (USA) and NINS (Japan), together with NRC (Canada) and NSC and ASIAA (Taiwan), in cooperation with



the Republic of Chile. The Joint ALMA Observatory is operated by ESO, AUI/NRAO and NAOJ. T.H. is supported by the MEXT/JSPS KAKENHI Grant Numbers 21224002, 24684011, and 25108005, and the

ALMA Japan Research Grant of NAOJ Chile Observatory, NAOJ-ALMA-0006. M.H. is supported by the MEXT/JSPS KAKENHI Grant Numbers 24540242 and 25120007.

## REFERENCES

- Alcolea, J., & Menten, K. M., in *Lecture Notes in Physics* 412, *Astrophysical Masers* (ed. Clegg, A. W. & Nedoluha, G. E., Springer) 399
- Allen, D. A. & Burton, M. G. 1993, *Nature*, 363, 54
- Bally, J., Cunningham, N. J., Moeckel, N., Burton, M. G., Smith, N., Frank, A., & Nordlund, A. 2011, *ApJ*, 727, 113
- Bally, J., Ginsburg, A., Silvia, D., & Youngblood, A. 2015, *A&A*, 579, A130
- Baudry, A., Herpin, F., & Lucas, R. 1998, *A&A*, 335, 654
- Beuther, H. & Nissen, H. D. 2008, *ApJL*, 679, L121
- Beuther, H., Zhang, Q., Reid, M. J., et al. 2006, *ApJ*, 636, 323
- Chatterjee, S., & Tan, J. C. 2012, *ApJ*, 754, 152
- Chen, P., Pearson, J. C., Pickett, H. M., Matsuura, S., & Blake, G. A. 2000, *ApJS*, 128, 371
- Churchwell, E., Felli, M., Wood, D. O. S., & Massi, M. 1987, *ApJ*, 321, 516
- Doeleman, S. S., Lonsdale, C. J., & Pelkey, S. 1999, *ApJ*, 510, L55
- Doeleman, S. S., Lonsdale, C. J., Kondratko, P. T., & Predmore, C. R. 2004, *ApJ*, 607, 361
- Favre, C., Despois, D., Brouillet, N., et al. 2011, *A&A*, 532, A32
- Friedel, D. N. & Widicus Weaver, S. L. 2011, *ApJ*, 742, 64
- Gaume, R. A., Wilson, T. L., Vrba, F. J., Johnston, K. J., & Schmid-Burgk, J. 1998, *ApJ*, 493, 940
- Genzel, R., Reid, M. J., Moran, J. M., & Downes, D. 1981, *ApJ*, 244, 884
- Goddi, C., Greenhill, L. J., Chandler, C. J., Humphreys, E. M. L., Matthews, L. D., & Gray, M. D. 2009, *ApJ*, 698, 1165
- Goddi, C., Humphreys, E. M. L., Greenhill, L. J., Chandler, C. J., & Matthews, L. D. 2011, *ApJ*, 728, 15
- Gómez, L., Rodríguez, L. F., Loinard, L., Lizano, S., Allen, C., Poveda, A., & Menten, K. M. 2008, *ApJ*, 685, 333
- Greenhill, L. J., Gezari, D. Y., Danchi, W. C., et al. 2004, *ApJL*, 605, L57
- Greenhill, L. J., Gwinn, C. R., Schwartz, C., Moran, J. M., & Diamond, P. J. 1998, *Nature*, 396, 650
- Greenhill, L. J., Reid, M. J., Chandler, C. J., Diamond, P. J., & Elitzur, M. 2004, in *IAU Symp. 221, Star Formation at High Angular Resolution*, ed. M. Burton, R. Jayawardhana, T. Bourke (San Francisco, CA: ASP), 155
- Greenhill, L. J., Goddi, C., Chandler, C. J., Matthews, L. D., & Humphreys, E. M. L. 2013, *ApJ*, 770, 32
- Hirota, T., Tsuboi, M., Fujisawa, K. et al. 2011, *ApJ*, 739, L59
- Hirota, T., Kim, M. K., & Honma, M. 2012, *ApJL*, 757, L1
- Hirota, T., Bushimata, T., Choi, Y. K. et al. 2007, *PAJS*, 59, 897
- Hirota, T., Kim, M. K., Kurono, Y., & Honma, M. 2014a, *ApJL*, 782, L28
- Hirota, T., Tsuboi, M., Kurono, Y., et al. 2014b, *PASJ*, 66, 106
- Hirota, T., Kim, M. K., Kurono, Y., & Honma, M. 2015, *ApJ*, 801, 82
- Humphreys, E. M. L. 2007, in *IAU Symp. 242, Astrophysical Masers and their Environments*, ed. J. M. Chapman & W. A. Baan (Cambridge: Cambridge Univ. Press), 471
- Hunter, T. R., Young, K. H., Christensen, R. D., & Gurwell, M. A. 2007, in *IAU Symp. 242, Astrophysical Masers and Their Environments* (Cambridge: Cambridge Univ. Press), 481
- Kaifu, N., Usuda, T., Hayashi, S. S., et al. 2000, *PASJ*, 52, 1
- Kleinmann, D. E. & Low, F. J. 1967, *ApJL*, 149, L1
- Kim, M. K., Hirota, T., Honma, M., et al. 2008, *PASJ*, 60, 991
- Matthews, L. D., Greenhill, L. J., Goddi, C., Chandler, C. J., Humphreys, E. M. L., & Kunz, M. W. 2010, *ApJ*, 708, 80
- Menten, K. M., & Reid, M. J. 1995, *ApJ*, 445, L157
- Menten, K.M., Reid, M. J., Forbrich, J., & Brunthaler, A. 2007, *A&A*, 474, 515
- Menten, K. M. & Young, K. 1995, *ApJL*, 450, L67
- Menten, K. M., Philipp, S. D., G'usten, R., Alcolea, J., Polehampton, E. T., & Br'unken, S. 2006, *A&A*, 454, L107
- Morita, K., Hasegawa, T., Ukita, N., Okumura, S., & Ishiguro, M. 1992, *PASJ*, 44, 373
- Niederhofer, F., Humphreys, E. M. L., & Goddi, C. 2012a, *A&A*, 548, A69
- Niederhofer, F., Humphreys, E., Goddi, C., & Greenhill, L. J. 2012b, in *IAU Symp. 287, Cosmic Masers -from OH to H<sub>2</sub>O*, (Cambridge: Cambridge Univ. Press), 184
- Nesterenok, A. V. 2015, *MNRAS*, 449, 2875
- Neufeld, D. A., Wu, Y., Kraus, A., et al. 2013, *ApJ*, 769, 48
- Patel, N. A., Curiel, S., Zhang, Q., Sridharan, T. K., Ho, P. T. P., & Torrelles, J. M. 2007, *ApJ*, 658, L55
- Plambeck, R. L., Wright, M. C. H., Carlstrom, J. E. 1990, *ApJ*, 348, L65
- Plambeck, R. L., Wright, M. C. H., Friedel, D. N., et al. 2009, *ApJL*, 704, L25
- Plambeck, R. L., Bolatto, A. D., Carpenter, J. M., et al. 2013, *ApJ*, 765, 40
- Reid, M. J., Menten, K. M., Greenhill, L. J., & Chandler, C. J. 2007, *ApJ*, 664, 950
- Richards, A. M. S., Impellizzeri, C. M. V., Humphreys, E. M., et al. 2014, *A&A*, 572, L9
- Schilke, P., Benford, D. J., Hunter, T. R., Lis, D. C., & Phillips, T. G. 2001, *ApJS*, 132, 281
- Sitarski, B. N., Morris, M. R., Lu, J. R., et al. 2013, *ApJ*, 770, 134
- Tan, J. C. 2004, *ApJL*, 607, L47
- Testi, L., Tan, J. C., & Palla, F. 2010, *A&A*, 522, A44
- Wright, M. C. H., Plambeck, R. L., Mundy, L. G., & Looney, L. W. 1995, *ApJ*, 455, L185
- Zapata, L. A., Menten, K., Reid, M., & Beuther, H. 2009a, *ApJ*, 691, 332
- Zapata, L. A., Loinard, L., Schmid-Burgk, J., Rodríguez, L. F., Ho, P. T. P., & Patel, N. A. 2011, *ApJ*, 726, L12
- Zapata, L. A., Schmid-Burgk, J., Ho, P. T. P., Rodríguez, L. F., & Menten, K. M. 2009b, *ApJL*, 704, L45
- Zapata, L. A., Rodríguez, L. F., Schmid-Burgk, J., Loinard, L., Menten, K. M., & Curiel, S. 2012, *ApJ*, 754, L17